Temperature dependence and temporal dynamics of Mn^{2+} upconversion luminescence sensitized by Yb^{3+} in codoped $LaMgAl_{11}O_{19}$

R. Martín-Rodríguez,[1] R. Valiente,[1] F. Rodríguez,[2] F. Piccinelli,[3] A. Speghini,[3] and M. Bettinelli[3]

[1]*MALTA Consolider Team, Depto. Física Aplicada, Facultad de Ciencias, Universidad de Cantabria, Avda. de Los Castros s/n, 39005 Santander, Spain*

[2]*MALTA Consolider Team, Depto. CITIMAC, Facultad de Ciencias, Universidad de Cantabria, Avda. de Los Castros s/n, 39005 Santander, Spain*

[3]*Laboratory Chimica dello Stato Solido, DB, INSTM, Università di Verona, UdR Verona, Ca' Vignal, Strada Le Grazie 15, I-37134 Verona, Italy*

(Received 14 April 2010; revised manuscript received 18 June 2010; published 11 August 2010)

A detailed spectroscopic study of the upconversion properties in Mn^{2+}-Yb^{3+} codoped $LaMgAl_{11}O_{19}$ is presented. Pulsed and continuous-wave infrared excitation in the $^2F_{7/2} \rightarrow {}^2F_{5/2}$ Yb^{3+} absorption peaks induces broad Mn^{2+} green emission at 19450 cm^{-1}, which is assigned to the $^4T_1 \rightarrow {}^6A_1$ transition in tetrahedral Mn^{2+} and sharp peaks associated with Yb^{3+}-pairs luminescence. Both emissions have very different temporal evolution and can be separated by time-resolved spectroscopy. Among the different concentrations under investigation, the 2%Mn^{2+}-5%Yb^{3+} codoped system presents the highest upconversion efficiency. The corresponding emission remains visible to the naked eye up to 650 K. The time dependence of the Mn^{2+} luminescence upon Yb^{3+} excitation shows distinct behaviors for different doping concentrations. The temporal evolution of the intensity for the diluted system doped with 2%Mn^{2+} and 5%Yb^{3+} together with the pure manganese compound doped with 1%Yb^{3+}, as well as the temperature dependence of the upconversion emission intensity and lifetime are relevant to identify the underlying upconversion mechanisms. We show that the main processes responsible for upconversion in this doubly transition-metal rare-earth doped oxide are both ground-state absorption (GSA)/excited-state absorption and GSA/energy-transfer upconversion. An analysis of these processes yielding highly efficient luminescence is discussed on the basis of crystal structure and dopants.

DOI: 10.1103/PhysRevB.82.075117 PACS number(s): 78.55.−m, 78.47.−p, 71.55.−i, 61.05.cp

I. INTRODUCTION

The attention on upconversion (UC) processes in which ultraviolet-visible light is generated upon infrared (IR) excitation is increasing because of their applications in bioimaging, display phosphors, lasers, or efficiency improvement of bifacial solar cells.[1–3] The most relevant UC mechanisms are ground-state absorption/excited-state absorption (GSA/ESA), energy-transfer upconversion (GSA/ETU), cooperative luminescence, cooperative sensitization and photon avalanche processes.[4,5] The majority of UC studies investigated up to date have involved combinations of rare-earth (RE) ions. In particular, Yb^{3+} has been extensively used as a sensitizer due to the relatively high oscillator strength of the $^2F_{7/2} \rightarrow {}^2F_{5/2}$ transition. This transition is located in the near infrared (NIR), just in the range of inexpensive laser diodes and is resonant with the energy levels of some other trivalent lanthanide ions. Opposite to *f-f* transitions in RE ions, *d-d* transitions of transition-metal (TM) ions are much more sensitive to the local environment and therefore, associated UC properties can be tuned by applying hydrostatic pressure,[6] and eventually by changing the crystal composition (internal or chemical pressure). In this sense, the combination of lanthanide and TM ions extends the UC luminescent tuning capability through changes in both energy resonances and emitting state energies.

The first demonstration of UC luminescence in TM-RE mixed systems was observed in Yb^{3+}-doped $CsMnCl_3$ and $RbMnCl_3$, and in Cr^{3+}-Yb^{3+} codoped $Y_3Ga_5O_{12}$, at low temperatures.[7,8] A GSA/ESA process between Mn^{2+}-Yb^{3+} dimer states was established as the main mechanism involved in the red UC luminescence in Yb^{3+}-doped $RbMnCl_3$ single crystal.[9] This host incorporates trivalent impurities as Mn^{2+}-Yb^{3+} pairs with charge compensation vacancies. The use of manganese hosts ensures clustering since an Yb^{3+} ion has always some Mn^{2+} ion as a near neighbor. The same model was proposed to explain both Mn^{2+} and Yb^{3+} pairs UC emission in Yb^{3+}-doped $CsMnBr_3$ single crystals.[10] Evidence of GSA/ETU between Mn^{2+}-Yb^{3+} dimers was found in Yb^{3+}-doped $CsMnCl_3$.[11] All these compounds show UC luminescence only at low temperature. It is well known that TM-concentrated compounds exhibit luminescence quenching as temperature increases. This phenomenon was explained by thermally activated excitation migration and subsequent transfer to nonradiative traps.[12] Therefore, the temperature-induced luminescence quenching is inherent to concentrated manganese systems and occurs independently of the excitation mechanism via NIR or directly into Mn^{2+} in the visible region.

Another difficulty in the UC luminescence investigation involves finding suitable host lattices able to accommodate both Mn^{2+} and Yb^{3+} at well-defined sites without charge compensation. $LaMgAl_{11}O_{19}$ (LMA) meets all these requirements. LMA crystallizes in the magnetoplumbite-type structure (hexagonal, $P6_3/mmc$ space group).[13] It consists of spinel blocks separated by an intermediate layer containing three oxygen ions, one lanthanum, and one aluminum per spinel block. Mg^{2+} ions are accommodated into the spinel blocks. LMA doped with Mn^{2+} is a well-known green phosphor, which can be excited by vacuum-ultraviolet radiation

and used in plasma display panels.[14] In Mn^{2+}-Yb^{3+} codoped LMA, Mn^{2+} ions occupy the tetrahedral Mg^{2+} sites whereas Yb^{3+} replaces La^{3+}. Recently, we have shown intense green UC luminescence in LMA codoped with 1%Mn^{2+}-1%Yb^{3+} upon Yb^{3+} $^2F_{7/2} \rightarrow {}^2F_{5/2}$ excitation, which persists up to 500 K.[15] Here, we present an extended spectroscopic investigation to clarify the effects of Mn^{2+} and Yb^{3+} concentrations and temperature on UC luminescence and lifetime. Experimental results are reported in order to clarify the UC mechanisms in Mn^{2+}-Yb^{3+} codoped LMA yielding Mn^{2+} luminescence after Yb^{3+} excitation and determine optimum doping concentrations to achieve the highest UC efficiency. We have selected three different Mn^{2+} and Yb^{3+} doping levels in order to cover all the aspects of the UC processes; LMA: 1%Mn^{2+}, 1%Yb^{3+} in which UC luminescence at high temperature was observed for the first time, LMA: 2%Mn^{2+}, 5%Yb^{3+} in which twice the Mn^{2+} concentration is used for Yb^{3+} in order to increase the UC efficiency and pure manganese lattice doped with 1%Yb^{3+} in order to ensure that every Yb^{3+} ion has always one Mn^{2+} ion as a near neighbor.

II. EXPERIMENTAL SECTION

Microcrystalline powders of LMA codoped with different nominal molar concentrations, 1%Mn^{2+}-1%Yb^{3+} and 2%Mn^{2+}-5%Yb^{3+} as well as 1%Yb^{3+}-doped $LaMnAl_{11}O_{19}$ (LMnA) were prepared by the precipitation method described elsewhere.[16] Briefly, stoichiometric amounts of $La(NO_3)_3 \cdot 5H_2O$, $Al(NO_3)_3 \cdot 9H_2O$, $Mg(NO_3)_2 \cdot 6H_2O$, $Mn(NO_3)_2 \cdot H_2O$, and $Yb(NO_3)_3 \cdot 5H_2O$ were dissolved in distilled water under stirring. Then aqueous NH_3 was added until a pH of 8.5 was reached and precipitation as hydroxides occurred. The hydroxides were centrifuged, washed with distilled water, and heated at 90 °C for 20 h. A final treatment at 700 °C for 2 h and 1500 °C for 1 h was carried out.

X-ray diffraction (XRD) measurements were carried out in a Thermo ARL X´TRA powder diffractometer, operating in the Bragg-Brentano geometry and equipped with a Cu-anode x-ray source (Kα, $\lambda = 0.15418$ nm), using a Peltier Si(Li) cooled solid-state detector. The powder patterns were collected in the 15°–85° 2θ range at a scan rate of 0.1°/min and a time of exposure of 10 s. Polycrystalline samples were ground in a mortar and then put in a low-background sample holder for data collection. Phase identification was performed with the PDF-4+ 2007 database provided by the International Centre for Diffraction Data. Rietveld structural refinement was further performed on all samples using MAUD program.[17]

Mn^{2+} photoluminescence and excitation spectra were measured upon excitation with a Xe lamp. Yb^{3+} emission, and Mn^{2+} and Yb^{3+}-pairs UC luminescence spectra were obtained by exciting with a continuous-wave laser diode emitting at 975 nm. The emission was detected by a Hamamatsu (R928) photomultiplier and all the samples were measured under identical conditions and detection geometry. An optical parametric oscillator system (Vibrant II, OPOTEK) was used for lifetime and time-resolved spectroscopy experiments upon excitation with 10 ns laser pulses at selected wavelengths. Two different setups were used for light intensity detection: a TRIAX monochromator (TRIAX 320) equipped with an intensified CCD (HORIBA iCCD-3553) and a single monochromator (CHROMEX 500IS/SM) with a Hamamatsu (R928) photomultiplier or an extended IR (R7102) photomultiplier together with a multichannel scaler (Stanford Research SR-430). Temperature-dependent measurements in the range 15–300 K were carried out in a closed-cycle helium cryostat (Air Products CS202E) whereas high-temperature experiments (300–650 K) were performed with a Leitz microscope heating stage. All spectra were corrected for instrumental response and therefore given in photons versus wavenumber.[18]

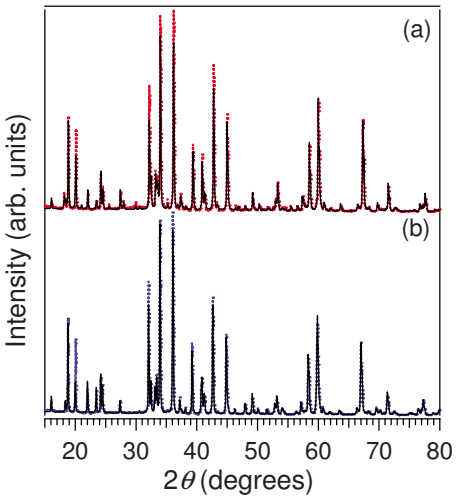

FIG. 1. (Color online) XRD patterns of (a) LMA: 2%Mn^{2+}, 5%Yb^{3+} and (b) LMnA: 1%Yb^{3+}. Colored dots show the experimental data and black lines the Rietveld refinements. The final R_w statistical indexes for the refinements are 13.8% for LMA: 2%Mn^{2+}-5%Yb^{3+} and 12.8% for LMnA: 1%Yb^{3+}.

III. RESULTS AND DISCUSSION

A. Crystal structure

XRD patterns of 2%Mn^{2+}-5%Yb^{3+} codoped LMA and 1%Yb^{3+}-doped LMnA are shown in Fig. 1. Both patterns indicate a fairly good crystallization of synthesized powders in the $PbFe_{12}O_{19}$ magnetoplumbite structure ($P6_3/mmc$ space group).[19] For the structural refinement the "vacancy model" published by Iyi *et al.*[20] on a lanthanum hexaaluminate compound was exploited.

The Rietveld refinement of the LMA: 2%Mn^{2+}, 5%Yb^{3+} XRD pattern is consistent with the magnetoplumbite structure with lattice parameters $a = 5.5602(5)$ Å and $c = 22.055(4)$ Å but also reveals small traces (4%, volume fraction) of Al_2O_3 (R-3c space group). The divalent ion occupies exclusively the 4f site (0.5 occupancy factor) together with an Al^{3+} ion and both ions are tetrahedrally coordinated by oxygens with a C_{3v} point symmetry.[13] For the LMnA powder containing Mn^{2+} ion instead of Mg^{2+} we obtain similar results; 97% of $LaMnAl_{11}O_{19}$ magnetoplumbite structure and small traces of Al_2O_3. Mn^{2+} ions also occupy only the 4f site (0.5 occupancy factor).[21] For this phase the refined cell parameters are: $a = 5.5818(5)$ and $c = 22.070(3)$ Å. The in-

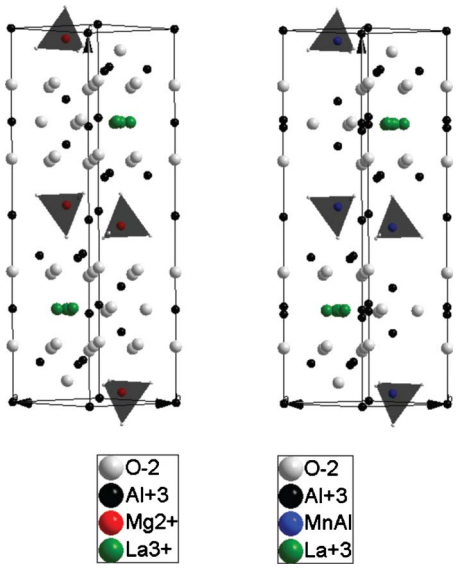

FIG. 2. (Color online) Unit cells for LMA (left) and LMnA (right) crystals. The tetrahedral coordination of Mg^{2+} or Mn^{2+} by oxygens is illustrated.

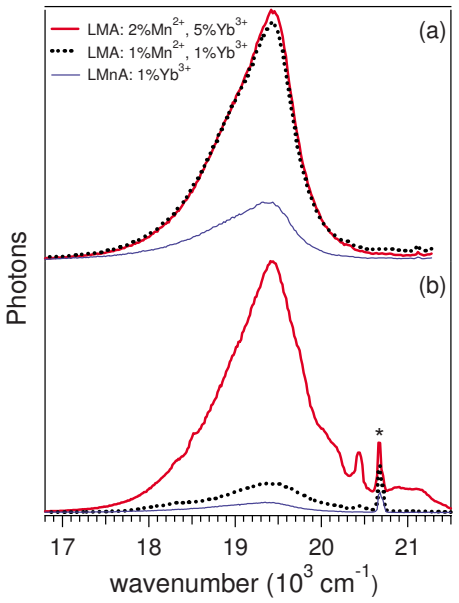

FIG. 3. (Color online) RT luminescence of Mn^{2+}-Yb^{3+} codoped LMA upon excitation at (a) 23580 cm^{-1} and (b) 10250 cm^{-1} for the following concentrations: 1%Mn^{2+}-1%Yb^{3+} (black-dotted line), 2%Mn^{2+}-5%Yb^{3+} (red-thick line) and pure manganese doped with 1%Yb^{3+} (blue-thin line). * is a laser artifact appearing at twice the excitation frequency. Measurements were carried out under the same experimental conditions.

creased cell parameters observed for LMnA in comparison with LMA reflect the bigger ionic radius of Mn^{2+} with respect to Mg^{2+}. The unit cells of the LMA and LMnA crystal structures are shown in Fig. 2. There are two different sites for the lanthanides in both LMA and LMnA phases. In the LMA sample the principal site (0.49 occupancy) has D_{3h} symmetry and a 12-fold coordination by oxygens whereas the satellite La site (0.115 occupancy) has a lower point symmetry (C_{2v}).[13] In the case of the LMnA compound, the satellite La site has the same point symmetry as in LMA, but with lower occupancy factor (0.05), whereas the principal La site is slightly shifted from the theoretical position (0.667, 0.333, and 0.25), with concomitant change in the point symmetry (from D_{3h} to C_s). In addition while the oxygen atoms show the same crystallographic sites occupation for both phases, light differences in the sublattice of Al^{3+} ions are detected. In particular, the sites with Wyckoff notation 12*k*, 4*f*, 2*a*, and 4*e* are populated with almost the same occupancy by Al^{3+} ions in both LMA and LMnA phases but only in the case of the former compound, one more 12*k* site is available for these ions (occupancy 0.0556). From our structural refinement the following distances are obtained: La(1)-Mg =5.844(1) Å and La(2)-Mg=5.728(3) Å for LMA and La(1)-Mn=5.795(2) Å and La(2)-Mn=5.724(4) Å for LMnA. The shortest La-La distance is 11.337(5) Å and 11.324(4) Å for LMA and LMnA, respectively. These distances are relevant for Mn^{2+}-Yb^{3+} interaction and the subsequent energy-transfer process.

B. Concentration dependence

Figure 3 compares the RT luminescence spectra of codoped LMA for different Mn^{2+} and Yb^{3+} concentrations upon visible and IR excitation. The green broad band emission is assigned to the Mn^{2+} $^4T_1 \rightarrow {}^6A_1$ transition in tetrahedral coordination and the high-energy peaks observed in the UC spectra are due to Yb^{3+}-Yb^{3+} cooperative luminescence.[15] No shift in energy or change in bandwidth is observed comparing the Mn^{2+} luminescence after direct and UC excitation. Considering the Mn^{2+} sensitivity to surrounding, this indicates that both direct and UC luminescence are originated from Mn^{2+} ions having the same environment, what is an indication of the homogenous distribution of Mn^{2+} and Yb^{3+} impurities in LMA. The green Mn^{2+} emission in LMA: 2%Mn^{2+}, 5%Yb^{3+} is centered at 19430 cm^{-1} (515 nm) while the same band appears about 50 cm^{-1} toward higher energy for LMnA: 1%Yb^{3+} according to expectations due to the smaller ionic radius of Mg^{2+} compared to Mn^{2+}.

It is worth noting that Mn^{2+} emission is obtained for all doping concentrations upon excitation in both 23580 cm^{-1} (424 nm) and 10250 cm^{-1} (976 nm) bands even above RT. For direct Mn^{2+} excitation [Fig. 3(a)], the RT luminescence intensity ratio of the pure manganese compound (LMnA) to the Mn^{2+}-doped LMA was found to be approximately 1:5 while the intensity for 1%Mn^{2+} and 2%Mn^{2+} compounds is roughly the same. This drastic reduction in emission intensity is ascribed to thermally activated energy migration and partial trapping into nonluminescent impurities as commonly occurs in concentrated manganese systems. Considering crystalline quality and emission efficiency, LMA codoped with 2%Mn^{2+} and 5%Yb^{3+} doping levels provides an optimum efficient UC system. Figure 3(b) shows that UC intensity in 2%Mn^{2+}-5%Yb^{3+} codoped LMA is about an order of magnitude higher than the UC in 1%Mn^{2+}-1%Yb^{3+} codoped LMA. An increase in Mn^{2+} concentration beyond 2% leads to a progressive UC decrease.

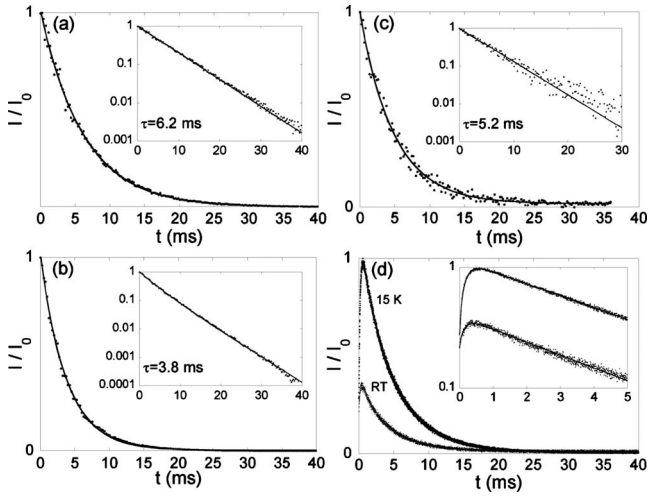

FIG. 4. RT temporal evolution of the normalized $^4T_1 \rightarrow {}^6A_1$ Mn^{2+} green luminescence intensity after pulsed excitation at 23580 cm^{-1} in (a) LMA: 2%Mn^{2+}, 5%Yb^{3+} and (b) LMnA: 1%Yb^{3+} and temporal behavior of the Mn^{2+} UC emission after pulsed excitation at 10205 cm^{-1} in (c) LMA: 2%Mn^{2+}, 5%Yb^{3+} at RT and (d) LMnA: 1%Yb^{3+} at both 15 K and RT. The insets show the same data in semilogarithmic scale. Continuous lines are the results of different fitting procedures (see text).

C. Temporal evolution

The temporal evolution of the RT Mn^{2+} $^4T_1 \rightarrow {}^6A_1$ green luminescence was recorded after direct Mn^{2+} excitation into the $^4A_1$, ^4E levels at 23580 cm^{-1} (424 nm) and IR excitation into the $^2F_{7/2} \rightarrow {}^2F_{5/2}$ Yb^{3+} transition at 10205 cm^{-1} (980 nm) with 10 ns short pulses for both LMA: 2%Mn^{2+}, 5%Yb^{3+} and LMnA: 1%Yb^{3+} samples (Fig. 4). The time-dependence intensity of the Mn^{2+} emission after visible excitation shows a single exponential decay with lifetimes of τ=6.2 ms for LMA: 2%Mn^{2+}, 5%Yb^{3+}, and τ=3.8 ms for LMnA: 1%Yb^{3+} [Figs. 4(a) and 4(b)]. However, the time dependence of the UC Mn^{2+} luminescence after IR excitation presents a different behavior in both systems. A single exponential decay (τ=5.2 ms) is observed in LMA: 2%Mn^{2+}, 5%Yb^{3+} [Fig. 4(c)]. This lifetime is significantly faster than the one obtained by direct Mn^{2+} excitation (τ=6.2 ms) as it was previously observed in Yb^{3+}-doped $RbMnCl_3$ (Ref. 9) and is probably related to an additional increase in emission probability due to the Mn^{2+}-Yb^{3+} interaction within the UC-efficient clusters. In the case of LMnA: 1%Yb^{3+}, a luminescence intensity rise before decaying is clearly detected [Fig. 4(d)]. These differences are crucial to identify the UC mechanism involved in these systems as will be discussed later.

Figures 5(a) and 5(b) show the temporal evolution of the Yb^{3+}-Yb^{3+} cooperative luminescence in LMA: 2%Mn^{2+}, 5%Yb^{3+} after IR excitation at 10205 cm^{-1} at 15 K and RT, respectively. The decay can be described by a single exponential function with lifetimes of τ=470 μs at 15 K and τ =220 μs at RT.

In LMA: 2%Mn^{2+}, 5%Yb^{3+} a lifetime of 5.2 ms has been obtained for the Mn^{2+} UC emission [Fig. 4(c)] while the RT lifetime of Yb^{3+}-Yb^{3+} cooperative luminescence is 220 μs

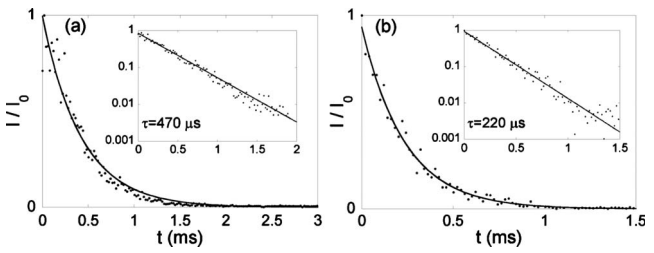

FIG. 5. Temporal behavior of the normalized Yb^{3+}-pairs emission in LMA: 2%Mn^{2+}, 5%Yb^{3+} after pulsed excitation at 10205 cm^{-1} at (a) 15 K and (b) RT. The insets show the same data in semilogarithmic scale.

[Fig. 5(b)]. Since both lifetimes differ by an order of magnitude, we can separate both UC emissions by time-resolved spectroscopy. Figure 6 shows both the Mn^{2+} green emission (broad band centered at 19430 cm^{-1}) and the Yb^{3+}-pairs luminescence (higher energy peaks above 19500 cm^{-1}) upon IR excitation at 10205 cm^{-1} taken at different delay times after the excitation pulse. It can be seen that the Yb^{3+}-Yb^{3+} cooperative emission intensity decreases much faster than the Mn^{2+} UC luminescence intensity according to their lifetimes. The figure clearly illustrates this phenomenon showing the rapid decay of Yb^{3+}-pairs luminescence on a millisecond time scale while the Mn^{2+} UC emission remains almost constant for this time.

D. Temperature dependence

Figure 7 shows the temperature dependence of the normalized emission intensity (I/I_{max}) and the lifetime (τ) of the Mn^{2+} $^4T_1 \rightarrow {}^6A_1$ transition in LMA: 2%Mn^{2+}, 5%Yb^{3+} and LMnA: 1%Yb^{3+} upon IR excitation at 10205 cm^{-1} in the range 15–600 K. It must be noted that for LMA: 2%Mn^{2+}, 5%Yb^{3+} the UC luminescence intensity remains almost constant up to RT. Although above this temperature the quenching process becomes important and the UC luminescence intensity starts to decrease, it still persists up to 600 K. The associated UC lifetime follows a similar trend; it diminishes slightly from 10 to 300 K and steeply decreases above this

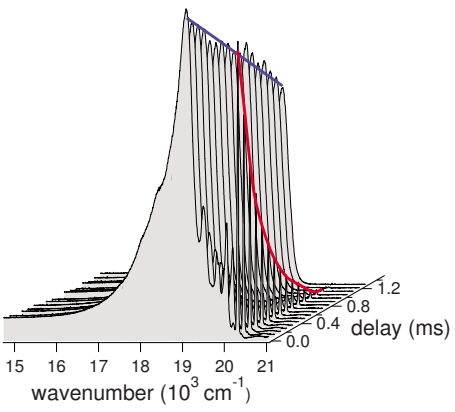

FIG. 6. (Color online) 15 K UC time-resolved emission of LMA: 2%Mn^{2+}, 5%Yb^{3+} upon pulsed IR excitation at 10205 cm^{-1} using different delay times after the excitation pulse.

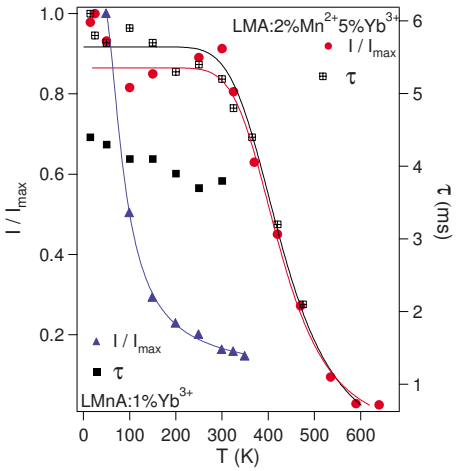

FIG. 7. (Color online) Temperature dependence of the LMA: 2%Mn^{2+}, 5%Yb^{3+} Mn^{2+} UC luminescence intensity (red circles) and Mn^{2+} UC emission lifetime (open squares) and temperature dependence of the LMnA: 1%Yb^{3+} Mn^{2+} UC luminescence intensity (blue triangles) and UC emission lifetime (black squares) after 10205 cm^{-1} excitation. Fits according to Eqs. (1)–(3) (see text) are also shown.

temperature. Both the intensity and the lifetime have a similar behavior pointing out the nonradiative character of the UC luminescence decrease. The quenching process of the Mn^{2+} UC luminescence is rather different in LMnA: 1%Yb^{3+}, as is shown in Fig. 7. As it usually happens in concentrated materials, the Mn^{2+} emission is thermally quenched at much lower temperatures ($T<100$ K) than in Mn^{2+} diluted samples. This is an intrinsic behavior of concentrated manganese and is usually accompanied by a similar lifetime decrease with temperature.[12,22] However, since in this case lifetime remains pretty constant until RT, the reduction in the intensity due to migration and subsequent quenching is unlikely. Instead, the photoluminescence dwindle above 100 K, which is induced either by direct excitation into the Mn^{2+} $^4A_1$ ^4E state or via UC in LMnA: 1%Yb^{3+}, must be ascribed to a decrease in the effective Mn^{2+} excitation with temperature. As we show below, this puzzling $I(T)$ behavior between 0 and 300 K can be phenomenologically described through a thermal activation processes for Mn^{2+} excitation.

In order to model the Mn^{2+} luminescence in LMA: 2%Mn^{2+}, 5%Yb^{3+} let us assume that the radiative lifetime, τ_R, does not change significantly with temperature. According to a model proposed by Mott,[23] thermally activated nonradiative processes can be described by an activation energy, E_a, with a pre-exponential frequency factor, p. Consequently, the lifetime and intensity dependences on temperature have been fitted according to Eqs. (1) and (2). In both cases the fitted parameters are $E_a=0.26$ eV and $p=180\times10^3$ s^{-1} for LMA: 2%Mn^{2+}, 5%Yb^{3+}.

$$\tau(T)=\frac{1}{\frac{1}{\tau_R}+pe^{-E_a/K_BT}}, \tag{1}$$

$$\frac{I(T)}{I_{max}}=\frac{1}{1+p\cdot\tau_R e^{-E_a/K_BT}}. \tag{2}$$

It must be noted that this simple model explains why $I(T)$ and $\tau(T)$ behave with temperature in the same manner. The activation energy ($E_a=0.26$ eV) and the Mn^{2+} dilution both suggest that the nonradiative process is associated with multiphonon relaxation within (MnO_4) units.

In this analysis we assume that the concentration of excited Mn^{2+} via UC or by direct excitation $^6A_1\rightarrow{}^4A_1$ ^4E is approximately independent on temperature. Nevertheless, in the case of LMnA: 1%Yb^{3+}, Eq. (2) must account for the fraction of excited Mn^{2+} as a function of temperature: $E_R(T)=[Mn](T)/[Mn](0)$ with [Mn] being the concentration of excited Mn^{2+}. Hence, Eq. (2) transforms to

$$\frac{I(T)}{I_{max}}=\frac{E_R(T)}{1+p\cdot\tau_R e^{-E_a/K_BT}}. \tag{3}$$

On the assumption that the concentration of up-converted Mn^{2+} does not change with temperature ($E_R=1$) then we obtain the same variation for $I(T)$ and $\tau(T)$ as Eqs. (1) and (2). However, this is not the case if E_R varies with temperature. The $I(T)$ reduction above 100 K observed in LMnA: 1%Yb^{3+} keeping $\tau(T)$ constant up to RT can be explained through this model if we consider that Mn^{2+} excitation is thermally deactivated: $E_R=(1-\alpha e^{-\Delta/K_BT})$, where Δ is the activation energy and α is the pre-exponential factor. Experimental $I(T)$ data (blue triangles) behaves in this way for values of $\Delta=5.6$ meV and $\alpha=1.2$.

Although the present model makes it compatible the reduction in intensity and the lifetime constancy, this thermal behavior is unusual for Mn^{2+} concentrated systems in which $I(T)$ correlates with $\tau(T)$. The microscopic origin of this puzzling phenomenon is unclear and deserves further investigation.

E. UC mechanism

The RT Mn^{2+} $^4T_1\rightarrow{}^6A_1$ UC luminescence intensity versus the excitation power density at 10250 cm^{-1} for LMA: 2%Mn^{2+}, 5%Yb^{3+} is plotted on a double-logarithmic scale in Fig. 8. This system presents a quadratic power dependence below 1.5 W cm^{-2} which is the typical behavior of a two-photon excitation process. The slope decreases from 2 to 1.5 at higher excitation power densities as explained elsewhere.[24,25] Since excitation occurs into $^2F_{5/2}$ Yb^{3+} states and emission takes place from $^4T_1$ Mn^{2+} states, the active UC mechanism in LMA: 2%Mn^{2+}, 5%Yb^{3+} and LMnA: 1%Yb^{3+} must involve participation of both Yb^{3+} and Mn^{2+} ions. Since Mn^{2+} has no intermediate resonant states with Yb^{3+}, then GSA/ESA and GSA/ETU mechanisms in pure ions must be ruled out in these systems. A simple model based on exchange-coupled Mn^{2+}-Yb^{3+} dimer states has been previously proposed to explain the experimental behavior in Yb^{3+}-doped $RbMnCl_3$, $CsMnBr_3$, and $CsMnCl_3$,[7,9] (see above).

The UC emission in LMA: 2%Mn^{2+}, 5%Yb^{3+} [Fig. 4(c)] shows an immediate decay after the laser pulse with no rise due to energy transfer longer than 80 ns (low-detection

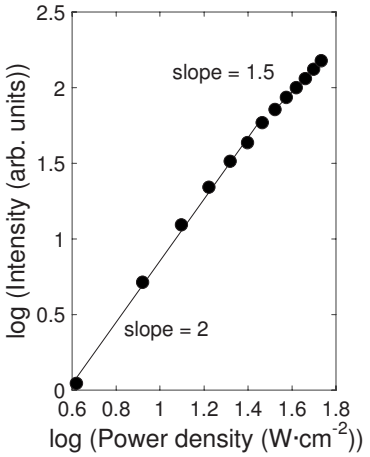

FIG. 8. Excitation power-density dependence of the RT Mn^{2+} UC emission in LMA: 2%Mn^{2+}, 5%Yb^{3+} upon excitation with a laser diode at 10250 cm^{-1}.

limit). According to the LMA crystal structure (Fig. 2), the Mn^{2+}-O-O′-Yb^{3+} dimers in LMA: 2%Mn^{2+}, 5%Yb^{3+} exhibits a superexchange pathway with shortest Mn^{2+}-Yb^{3+} distances of 5.728 Å.[26,27] Taking into consideration a GSA/ESA-type mechanism in Mn^{2+}-Yb^{3+} dimers, the GSA step is predominantly a single-ion process in Yb^{3+} but the ESA step requires the mixing of Mn^{2+} and Yb^{3+} states. The rise of the emission intensity after the excitation pulse in LMnA: 1%Yb^{3+} [Fig. 4(d)] evidences the contribution of some nonradiative energy-transfer process after the pulse to the UC mechanism. The involved processes can be GSA/ETU in a dimer or cooperative sensitization. Again, the Mn^{2+}-Yb^{3+} distance in LMnA (5.724 Å) is short enough to allow dimer formation, hence we propose the GSA/ETU as the actual mechanism. The Mn^{2+} lifetime is shorter in LMnA: 1%Yb^{3+} than in LMA: 2%Mn^{2+}, 5%Yb^{3+}, this evidences a larger exchange contribution for the pure manganese system. The fact that the intensity rise does not start from zero is noteworthy. This implies that there must be an additional excitation within the duration of the laser pulse governed by a GSA/ESA mechanism. Considering that the lifetime of the $^2F_{7/2}$-$^4T_1$ dimer state is approximately the same as the Mn^{2+} lifetime after direct excitation, it is possible to estimate the GSA/ESA and GSA/ETU contribution to the total intensity.[11,28] At 15 K about 23% of the total upconversion luminescence is due to excitation within the pulse (GSA/ESA) while contributions of 33% and 67% have been obtained at RT for GSA/ESA and GSA/ETU mechanisms, respectively.

Figure 9 shows a schematic representation of an exchange-coupled Mn^{2+}-Yb^{3+} dimer and an Yb^{3+} nearby monomer along with the proposed mechanisms for the UC luminescence; GSA/ESA for LMA: 2%Mn^{2+}, 5%Yb^{3+} and both GSA/ESA and GSA/ETU for LMnA: 1%Yb^{3+}. The dimer ground state and intermediate state are dominantly localized on Yb^{3+}. The higher excited states are mainly localized on Mn^{2+} ions.[9]

The temporal evolution of the LMnA: 1%Yb^{3+} can be simulated considering GSA/ESA and GSA/ETU mechanisms according to the five levels system shown in Fig. 10 involving an Yb^{3+} ion and a Mn^{2+}-Yb^{3+} dimer. Within this model the coupled differential rate equations describing the population of each level, N_i can be written as

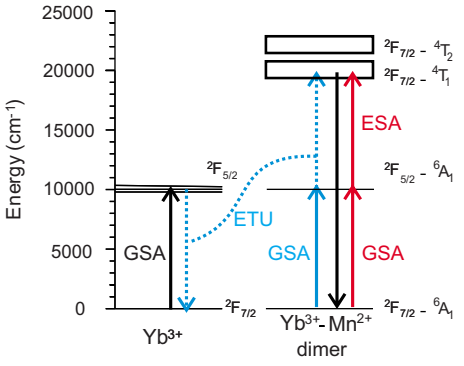

FIG. 9. (Color online) Energy states in a Mn^{2+}-Yb^{3+} dimer notation with the Mn^{2+} emission and the proposed UC mechanisms.

$$\frac{dN_0}{dt} = -GN_0 + k_1N_1 + W_{ETU}N_1N_3,$$

$$\frac{dN_1}{dt} = GN_0 - k_1N_1 - W_{ETU}N_1N_3,$$

$$\frac{dN_2}{dt} = -GN_2 + k_3N_3 + k_4N_4,$$

$$\frac{dN_3}{dt} = GN_2 - k_3N_3 - EN_3 + k_{43}N_4 - W_{ETU}N_1N_3,$$

$$\frac{dN_4}{dt} = EN_3 - k_{43}N_4 + W_{ETU}N_1N_3 - k_4N_4,$$

where k_i represents the decay rate of each level N_i, G, and E are the power-dependent GSA and ESA rate constants, respectively, and W_{ETU} is the two-center energy-transfer process parameter. k_1 and k_3 are known from the experimentally measured Yb^{3+} lifetime; 940 μs at 15 K and 370 μs at RT, which are significantly longer than those obtained for LMA: 2%Mn^{2+}, 5%Yb^{3+}, while k_4 is the inverse of Mn^{2+} emission

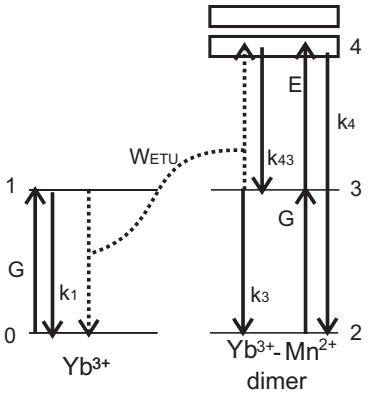

FIG. 10. Relevant levels involved in the GSA/ESA and GSA/ETU UC processes in LMnA: 1%Yb^{3+}.

lifetime; 4.4 ms at 15 K and 3.8 ms at RT. By fitting the time-dependent evolution of the UC luminescence in LMnA: 1%Yb^{3+} to this set of equations [Fig. 4(d)], we obtain the following energy-transfer rates, W_{ETU}, 2310 s^{-1} at RT and 3125 s^{-1} at 15 K, respectively. Nevertheless, the variation in the UC intensity depicted in Fig. 4(d) can be rationalized in terms of the transition rates of Mn^{2+} and Yb^{3+}. In fact, the rate equation for $N_4(t \geq 0)$ can be solved analytically on the assumption that Yb^{3+} populations, N_1 and N_3, are similar ($N_1 \approx N_3$), both decaying as $N_3 = N_3^0 e^{-w_3 t}$, where w_3 is a mean Yb^{3+} transition rate. This approximation yields a time-dependent Mn^{2+} population as $N_4 = N_4^0(e^{-kt} - \alpha e^{-2w_3 t})$ The parameter $k = k_4 + k_{43}$, governing the temporal decay of Fig. 4(d), is directly related to the Mn^{2+} transition rate whereas parameter w_3 controls the intensity rise immediately after $t = 0$. The parameters α and N_4^0 determines the Mn^{2+} population at $t=0$ due to GSA/ESA. This equation properly describes the I(t) behavior of Fig. 4(d) with fit parameters: $k = 238$ s^{-1} and $w_3 = 1043$ s^{-1} at RT and $k = 213$ s^{-1} and $w_3 = 2295$ s^{-1} at 15 K. Their reciprocal values are similar to the Mn^{2+} and Yb^{3+} lifetimes, respectively, what supports the proposed UC scenario of Mn^{2+} pumping via two Yb^{3+} ions, hence the involvement of GSA/ETU in LMnA: 1%Yb^{3+}.

IV. CONCLUSIONS

In this paper, the spectroscopic properties of LMA doped with different Mn^{2+} and Yb^{3+} concentrations indicate that these systems are very efficient for UC luminescence in Mn^{2+}. LMA crystallizes with the magnetoplumbite crystal structure where Mn^{2+} ions are tetrahedrally coordinated by oxygen atoms. UC Mn^{2+} luminescence and Yb^{3+}-pairs emission have been detected in all samples. We demonstrate that UC luminescence takes place via GSA/ESA mechanism for LMA: 2%Mn^{2+}, 5%Yb^{3+} whereas an additional GSA/ETU contribution participates in LMnA: 1%Yb^{3+}. This conclusion is based on time-resolved spectroscopy and impurity concentration dependent experiments. In both LMA and LMnA systems the luminescence via UC is observed up to RT and above 500 K in LMA: 2%Mn^{2+}, 5%Yb^{3+}, the latter UC emission being an order of magnitude stronger than in any other. It remains very intense up to RT but at higher temperatures both the emission intensity and lifetime decrease in a similar manner pointing out the nonradiative character of the quenching. A multiphonon relaxation process within MnO_4 is likely. In LMnA: 1%Yb^{3+} we detected an unusual decrease in the Mn^{2+} luminescence above 100 K with a constant lifetime which is not ascribed to Mn^{2+} energy migration and subsequent quenching but to a dwindle of Mn^{2+} pumping efficiency. This puzzling behavior has not been observed so far and its unclear origin yet deserves to be clarified. The experimental results and the theoretical rate equations model confirm the different proposed UC mechanisms involving Mn^{2+}-Yb^{3+} dimer formation.

ACKNOWLEDGMENTS

This work was financially supported by the Spanish Ministerio de Ciencia e Innovación (Project No. MAT2008-06873-C02-01/MAT) and the MALTA-Consolider Ingenio 2010 (Reference No. CSD2007-00045). R.M.-R. thanks the Spanish MEC for a FPI research grant (Reference No. BES-2006-13359). The expert technical assistance of E. Viviani and J. A. Barreda-Argüeso is gratefully acknowledged.

[1] M. Nyk, R. Kumar, T. Y. Ohulchanskyy, E. J. Bergey, and P. N. Prasad, Nano Lett. **8**, 3834 (2008).
[2] E. Heumann, S. Bär, K. Rademaker, G. Huber, S. Butterworth, A. Diening, and W. Seelert, Appl. Phys. Lett. **88**, 061108 (2006).
[3] T. Trupke, A. Shalav, B. S. Richards, P. Würfel, and M. A. Green, Sol. Energy Mater. Sol. Cells **90**, 3327 (2006).
[4] F. Auzel, Acad. Sci., Paris, C. R. **262**, 1016 (1966).
[5] V. V. Ovsyankin and P. Feofilov, JETP Lett. **3**, 322 (1966).
[6] O. S. Wenger, G. M. Salley, R. Valiente, and H. U. Güdel, Phys. Rev. B **65**, 212108 (2002).
[7] R. Valiente, O. S. Wenger, and H. U. Güdel, Chem. Phys. Lett. **320**, 639 (2000).
[8] S. Heer, M. Wermuth, K. Krämer, and H. U. Güdel, Phys. Rev. B **65**, 125112 (2002).
[9] R. Valiente, O. S. Wenger, and H. U. Güdel, Phys. Rev. B **63**, 165102 (2001).
[10] P. Gerner, O. S. Wenger, R. Valiente, and H. U. Güdel, Inorg. Chem. **40**, 4534 (2001).
[11] R. Valiente, O. S. Wenger, and H. U. Güdel, J. Chem. Phys. **116**, 5196 (2002).
[12] B. Henderson and G. F. Imbusch, *Optical Spectroscopy of Inorganic Solids* (Clarendon Press, Oxford, 1989).
[13] S. C. Abrahams, P. Marsh, and C. D. Brandle, J. Chem. Phys. **86**, 4221 (1987).
[14] S. Nukuta and T. Onimaru, U.S. Patent No. 7,037,445 (2006).
[15] R. Martín-Rodríguez, R. Valiente, and M. Bettinelli, Appl. Phys. Lett. **95**, 091913 (2009).
[16] J. M. P. J. Verstegen, J. L. Sommerdijk, and J. G. Verriet, J. Lumin. **6**, 425 (1973).
[17] L. Lutterotti and S. Gialanella, Acta Mater. **46**, 101 (1998).
[18] E. Ejder, J. Opt. Soc. Am. **59**, 223 (1969).
[19] V. Adelskold, Ark. Kemi, Mineral. Geol. **12**, 29 (1938).
[20] N. Iyi, Z. Inoue, S. Takekawa, and S. Kimura, J. Solid State Chem. **54**, 70 (1984).
[21] M. Gasperin, M. C. Saine, A. Kahn, F. Laville, and M. Lejus, J. Solid State Chem. **54**, 61 (1984).
[22] M. N. Sanz-Ortiz and F. Rodríguez, J. Chem. Phys. **131**, 124512 (2009).
[23] N. F. Mott, Proc. R. Soc. London **A167**, 384 (1938).
[24] M. Pollnau, D. R. Gamelin, S. R. Lüthi, H. U. Güdel, and M. P. Hehlen, Phys. Rev. B **61**, 3337 (2000).
[25] J. F. Suyver, A. Aebischer, S. García-Revilla, P. Gerner, and H. U. Güdel, Phys. Rev. B **71**, 125123 (2005).
[26] J. Luzón, J. Campo, F. Palacio, G. J. McIntyre, and A. Millán, Phys. Rev. B **78**, 054414 (2008).
[27] M. P. Hehlen, A. Kuditcher, S. C. Rand, and S. R. Lüthi, Phys. Rev. Lett. **82**, 3050 (1999).
[28] R. Martín-Rodríguez, R. Valiente, C. Pesquera, F. González, C. Blanco, V. Potin, and M. C. Marco de Lucas, J. Lumin. **129**, 1109 (2009).